5

DYNAMIC MODELLING OF TRUCK CROSSING BRIDGE

5.1 INTRODUCTION

Bridge and truck dynamics are a significant source of inaccuracy in B-WIM systems (Section 3.5.1). This chapter presents the parameters that affect the bridge response and the passage of a truck over a bridge is modelled numerically. Some of this formulation will be taken as reference for the development of a dynamic B-WIM algorithm in Chapter 7. These are one-dimensional bridge and truck models while more sophisticated three-dimensional finite element models will be introduced in Chapter 6.

A key source of error for WIM systems is vehicle dynamics. There are two main movements:

- a body oscillation with a frequency between 1.5 Hz and 4.5 Hz, related to the stiffness of suspensions and sprung mass (vehicle body),
- an axle oscillation with a higher frequency (8 to 15 Hz), mainly related to the unsprung mass (wheels and axles) and tyre stiffness.

If a WIM system was able to measure the applied force for a full period of the lowest frequency, the problem would be overcome. The only existing system able to achieve a continuous record of the applied truck wheel forces for a sufficient length of time is a B-WIM system. However, the interaction between bridge and vehicle is a very complex system. Accordingly, the development of an accurate Bridge Weigh In Motion system requires an understanding of how roads and bridges are affected by the passing of vehicles. A lot of authors have studied the modelling of the dynamic response of bridges induced by moving vehicles. Recent progress has been made through research projects such as the OECD DIVINE (**D**ynamic **I**nteraction of **V**ehicle **In**frastructures **E**xperiment) programme and the Vehicle Infrastructure Interaction series of conferences, the fifth of which was held in Poland in September 1999.

The author has implemented the simulation of a four-degree of freedom two-axle vehicle running on a simply supported beam with road irregularities. Equations of motion can be set for the vehicle and the bridge. These equations are coupled due to the interaction forces existing at the contact points. This simple model makes possible the study of the influence of different bridge, truck and/or road profile parameters, a lot of which are not controllable or measurable in experimental trials. In addition, an eleven degree of freedom four-axle vehicle developed by Green et al (1995) is used to investigate the influence of the suspension type and road roughness. These numerical simulations will be used in Chapters 7 and 9 to assess the influence of dynamics on B-WIM accuracy.

5.2 PLANAR DYNAMIC MODELS

The dynamic characteristics of a beam and planar vehicle models are described. In these simplified models, torsional bridge vibration and vehicle roll motion are neglected.

5.2.1 Bridge

The bridge structure is modelled here as a simply supported beam. Its behaviour is governed by the following properties: Young's modulus (E), mass per unit length (μ), damping (ξ), second moment of area (I) and bridge length (L). The natural frequencies in Hz of the bridge are defined by Equation 5.1:

$$f_n = \left(\frac{n}{L}\right)^2 \frac{\pi}{2}\sqrt{\frac{EI}{\mu}} \quad ; \quad n = 1,2\ldots \tag{5.1}$$

If damping was neglected, final results would be somewhat exaggerated. The exact magnitude of damping can be determined only from experimental tests on the real structure. As long as the amplitude of free vibration decays exponentially, it may be assumed that viscous type damping can be used in the mathematical model of the system. The damping factor, ξ, is obtained by measuring the number of oscillations N between two non-consecutive strain peaks (u_N and u_1) and applying Equation 5.2:

$$\frac{\xi}{\sqrt{1-\xi^2}} = \frac{Ln(u_N - u_1)}{2\pi N} \tag{5.2}$$

In Figure 5.1, a damping factor ξ = 0.05 results from u_N = 0.1504, u_1= 0.7279 and N = 5. The values of the logarithmic decrement of damping ($\frac{Ln(u_N - u_1)}{N}$) for concrete bridges vary in the range [0.02,0.20] (Cantieni 1983, Narayanan & Roberts 1991).

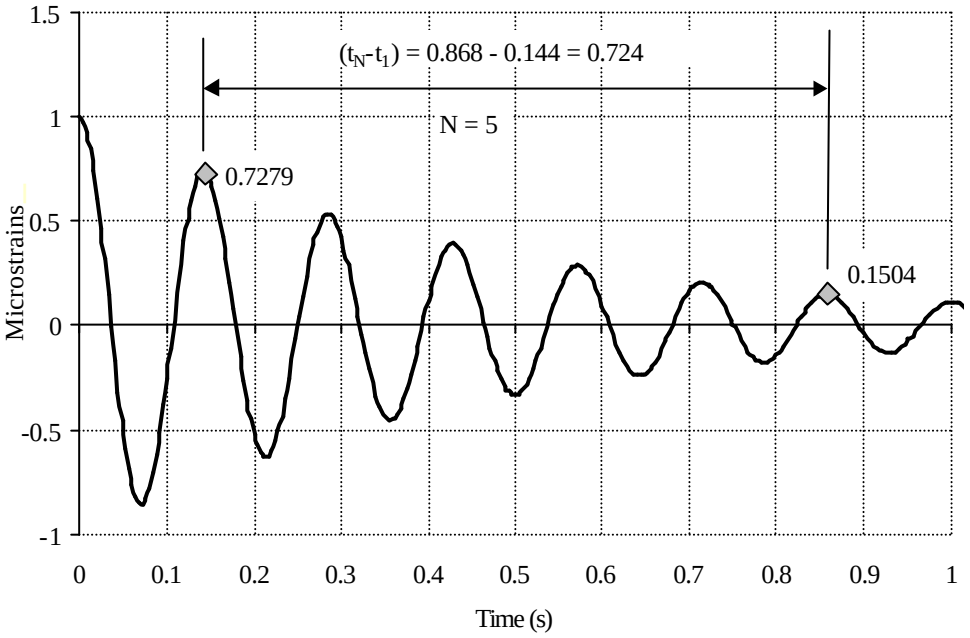

Figure 5.1 – Decay Record of Damped System

First damped frequency (f_d) is obtained by dividing the number of oscillations between two peaks (N) between their difference in time ($t_N - t_1$) (A peak in the spectrum of the record should confirm this value):

$$f_d = \frac{N}{t_N - t_1} \tag{5.3}$$

For the example in Figure 5.1, a damped frequency f_d = 7 Hz results from N = 5 and ($t_N - t_1$) = 0.724**.** The natural frequency of the bridge (f_n) is given by:

$$f_n = \frac{f_d}{\sqrt{1-\xi^2}} \tag{5.4}$$

where ξ is damping factor. For low values of damping, $f_n \cong f_d$. Bridges vary in natural frequency from 1 Hz to as high as 15 Hz (Cantieni 1983, Green et al. 1995). A further explanation of the relationships given in this section can be found in widely available structural dynamics books (Craig 1981, Clough & Penzien 1975, Nashif et al. 1985).

5.2.2 Truck

A truck is composed of body, suspension system and tyres. Mathematical models for these elements are defined below.

Static Model

The objective of a high-speed WIM system such as B-WIM is to achieve a degree of accuracy as close as possible to that given by a static scale. However, even for a vehicle stopped in a perfectly levelled site, static weights are influenced by vehicle mechanical parameters. When a load is applied normally to a tyre, the tyre deflects progressively as the load increases. The relationship between the load and deflection depends on the inflation pressure, and it is linear for a given inflation pressure, except at relatively low values of load, out of the range of practical interest (Wong 1993). Hence, the measured static weights depend on the compression of the springs of the suspension/tyre system.

If the springs are compressed differently and there are more than two axles (indeterminate structure), the real static weights can not be measured. In order to analyse this problem, a vehicle can be modelled as a sprung beam allowed to move vertically only at the axle locations. A simply supported beam would derive in the exact static axle weights due to equilibrium. Only in the case of an indeterminate structure –more than two axles–, there will be differences due to suspension springs if the supports are free to rotate. The gravity forces acting on the beam are due to a uniformly distributed mass per unit length, μ, and a concentrated mass, M (Figure 5.2).

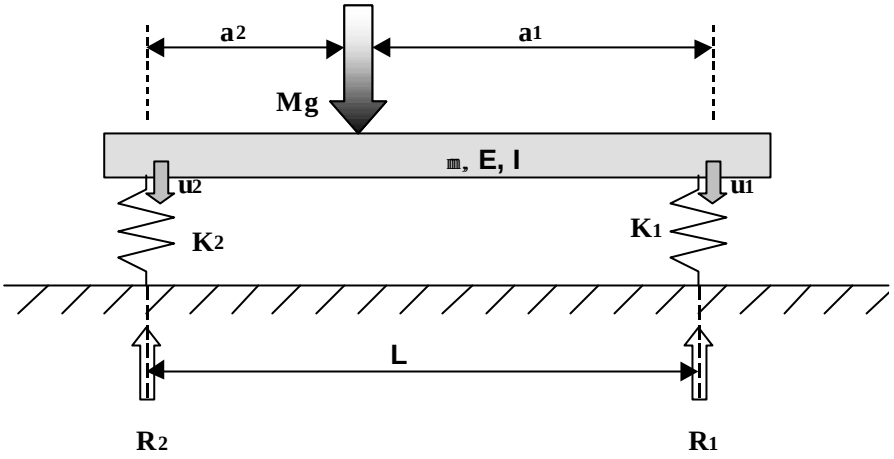

Figure 5.2 – Two-axle rigid vehicle idealised as a sprung beam

The problem is defined by the following parameters:

R_i : Static reaction at axle i (N),
K_i : Sprung stiffness corresponding to axle i (N/m),
a_i : Distance (m) from axle i to location of mass M,
μ : Mass per unit length (kg/m),
g : Acceleration of gravity (9.806 m/s^2),
E : Modulus of elasticity of the beam (N/m^2),
I : Second moment of area of the beam section (m^4),
M : Concentrated mass (kg),
L : Axle spacing (m),
u_i : Vertical displacement of axle i (m).

If the spring elements are ignored, the 'real' static axle weights W_1 and W_2 can be obtained from static equilibrium through Equations 5.5 and 5.6:

$$R_1 = \left(\frac{a_2}{L} M + \frac{\mu L}{2} \right) g \tag{5.5}$$

$$R_2 = \left(\frac{a_1}{L} M + \frac{\mu L}{2} \right) g \tag{5.6}$$

The stiffness matrix for the two degrees of freedom shown in Figure 5.2 is given by:

$$[K] = \begin{bmatrix} k_1 & 0 \\ 0 & k_2 \end{bmatrix} \tag{5.7}$$

The displacements of the springs at the front and rear axles are:

$$\begin{Bmatrix} u_1 \\ u_2 \end{Bmatrix} = \frac{1}{k_1 k_2} \begin{bmatrix} k_2 & 0 \\ 0 & k_1 \end{bmatrix} \begin{Bmatrix} \left(\frac{a_2}{L} M + \frac{\mu L}{2} \right) g \\ \left(\frac{a_1}{L} M + \frac{\mu L}{2} \right) g \end{Bmatrix} \tag{5.8}$$

These static displacements define the position of equilibrium of the vehicle. Measured vertical reactions (R_1 and R_2) depend on the displacements of the springs supporting the vehicle. The reactions at the front and rear axles are given by Equations 5.9 and 5.10:

$$R_1 = k_1 u_1 \tag{5.9}$$

$$R_2 = k_2 u_2 \tag{5.10}$$

Real (Equations 5.5 and 5.6) and measured static weights (Equations 5.9 and 5.10) give the same values as calculations correspond to a determinate structure. Minor differences will appear when there are more than two axles on the bridge. In this case, errors derived from measurements will depend on the load distribution, axle stiffness and beam stiffness. The results for the weight of an axle group or the whole vehicle can be improved by measuring all axles in one operation, as the differences in the compression of each spring compensate for each other (Equation 5.11).

$$\sum_{i=1}^{n} R_i = \sum_{i=1}^{n} W_i \tag{5.11}$$

where n is number of axles.

Tyres

In vehicle dynamics, the cushioning characteristics of a pneumatic tyre can be represented by a mass element and a linear spring (K_t) in parallel with a viscous damping element (C_t) representing the fundamental mode of vibration of the tyre (Figure 5.3).

The interaction force, R, between a tyre and the bridge is given by:

$$R = -(K_t z_t + C_t \frac{dz_t}{dt}) \tag{5.12}$$

where z_t is the displacement of the axle relative to the level of the road profile.

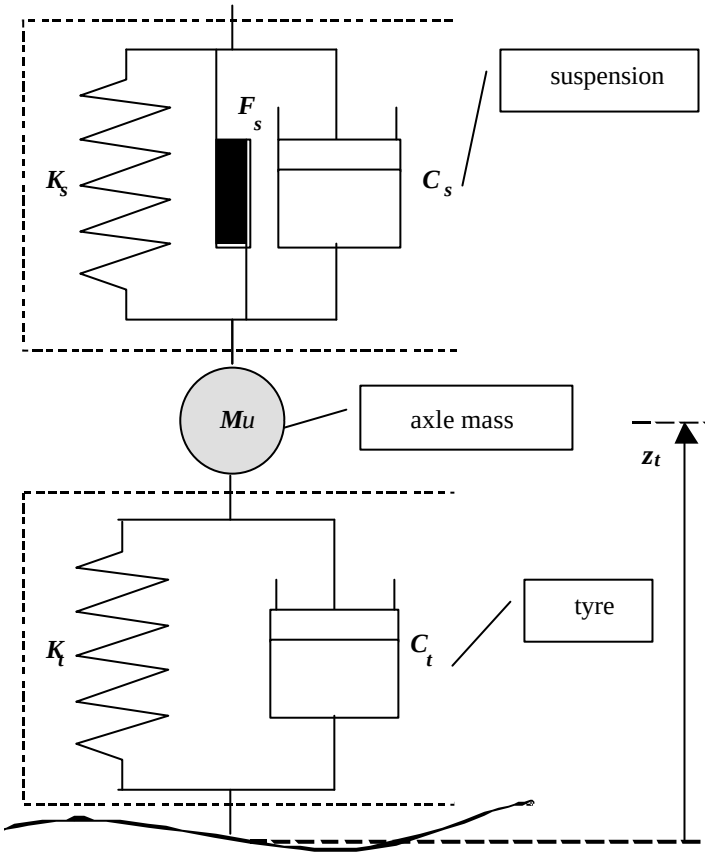

Figure 5.3 – Tyre and suspension idealisation

For a sample of truck tyres travelling at relatively low speed, Wong (1993) found that values of 'dynamic' vertical stiffness, K_t, vary between 764 and 1024 kN/m and stiffness of radial-ply tyres was generally lower than that of bias-ply tyres of similar size. This 'dynamic' vertical stiffness (i.e., that found by measuring the response of a rolling tyre to a known harmonic excitation) is preferred to the static vertical stiffness (from load-deflection curves) for simulation of vehicle dynamics. For heavy truck tyres, the dynamic

stiffness is generally approximately 5% less than the static stiffness, but values 26% lower than the static value have been reported for tractor tyres.

Wong shows that K_t decreases sharply as soon as the tyre begins rolling and the influence of speed becomes less important beyond a speed of approximately 20 km/h. The damping of a pneumatic tyre appears to be a combination of Coulomb-type and viscous-type damping, but an equivalent viscous damping factor, C_t, can be usually derived. Damping coefficient C_t drops rapidly as speed increases from 1 km/h to 5 km/h, after which an asymptote is reached. Further, dynamic stiffness K_t increases and damping coefficient C_t decreases with the inflation pressure.

Suspension

Figure 5.3 represents a simple model of a vehicle suspension system: A linear spring (K_s) is present in parallel with a linear viscous element of damping constant C_s and a Coulomb friction force F_s. The axial force S acting on the suspension system will be given by:

$$S = -\left(K_s z_s + C_s \frac{dz_s}{dt} + F_s \frac{dz_s/dt}{\left| dz_s/dt \right|} \right) \tag{5.13}$$

where z_s is the relative displacement between the axle and vehicle module.

However, the accuracy of this model is often unsatisfactory due to an overestimation of the response force (Kirkegaard et al. 1997). In practice, frequency and damping of the suspension are not independent parameters and it is difficult to design a suspension with effective damping above 2 Hz (OECD 1997). Section 5.6 introduces a more sophisticated suspension model based on data available from an instrumented truck.

Figure 5.4 illustrates types of mechanical behaviour that can be found as part of a suspension/tyre system. Figure 5.4(a) represents a linear spring with viscous damping where the damping force is proportional to the velocity of motion. Figure 5.4(b) represents Coulomb-damping friction, which is the result of sliding vibration bodies on a dry surface. A maximum force F_s equal to the applied force normal to the surface multiplied by the

coefficient of kinetic friction of the surface material is developed. Figure 5.4(c) represents other frictional forces with non-linear behaviour.

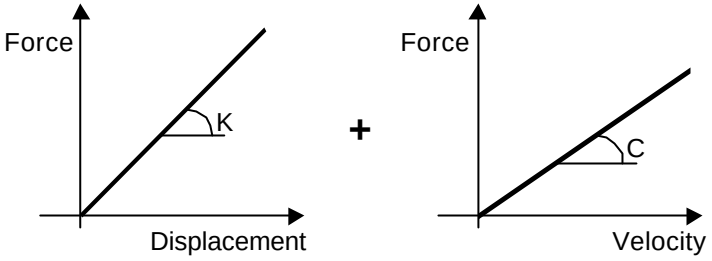

(a) Linear spring with viscous damping

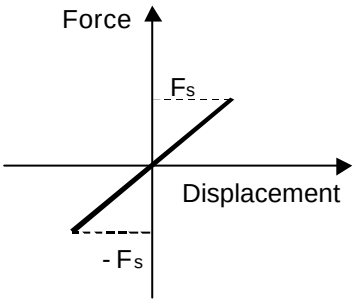

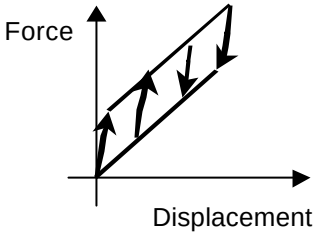

(b) Spring with Coulomb damping (c) Spring with non-linear behaviour

Figure 5.4 – Mathematical models for suspension/tyre elements

Body

The vehicle body is represented by a concentrated mass subjected to rigid-body motions. Two degrees of freedom are considered: vertical motion (z) and pitching rotation (φ). The dynamic characteristics of the body are mass moment of inertia of rotation (J) and body mass (M). Mass moment of inertia can be calculated from the weight distribution and dimensions of the body. In the case of a tractor-trailer configuration (Figure 5.5), the two modules are assumed to be linked together at a hinge.

Apart from the dynamic equations of equilibrium (Equations 5.13 to 5.16), it is necessary to set compatibility conditions between the relative displacements of each component (z_{t1}, z_{t2},..,z_{ti},..,z_{tn} as relative displacements of the i^{th} axle relative to the mean level of the surface irregularities, z_{s1},z_{s2},..,z_{si},..,z_{sn} as relative displacements between the i^{th} axle and the module, z_1, z_2, φ_1 and φ_2). These additional equations are based on the location of each degree of

freedom, rigid body translations in the x and z directions and rotations at the centres of gravity of the tractor and trailer.

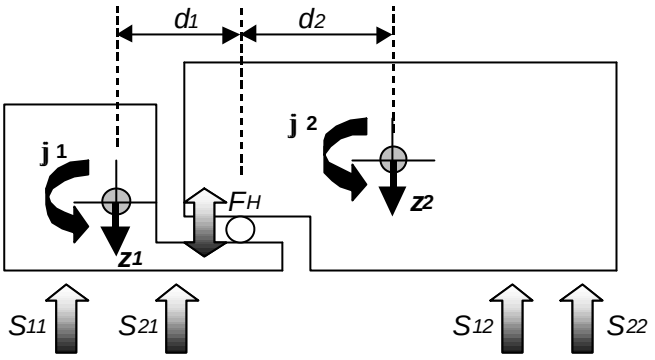

Figure 5.5 – Simplified Tractor + trailer body mass model

This hinge only allows a vertical force, F_H, to be transmitted between the modules. The equations of dynamic equilibrium for each module are:

$$M_j \frac{d^2 z_j}{dt^2} = \sum_{i=1}^{n_j} S_{ij} + F_H \quad ; \; j = 1,2 \tag{5.14}$$

$$J_j \frac{d^2 \varphi_j}{dt^2} = -(\sum_{i=1}^{n_j} S_{ij} l_{ij} + F_H d_j) \quad ; \; j = 1,2 \tag{5.15}$$

where

z_j : Vertical displacement of module j,

φ_j : Rotation of module j,

S_{ij} : Forces acting on the axle suspensions supporting the module j,

l_{ij} : Distance from axle i in module j to the mass centre of gravity of module j,

d_j : Distance from the hinge to the mass centre of gravity of module j,

M_j : Mass of module j,

n_j : Number of axles supporting module j,

J_j : Mass moment of inertia of rotation of module j.

5.3 BRIDGE SUBJECTED TO A MOVING CONSTANT LOAD

This section introduces the case of a moving load that exerts a constant force on a beam. The distributed mass of the beam will be taken into account, but the mass of the load itself is omitted.

5.3.1 Single load

A moving load *R*, acting downwards on a beam and moving from left to right at a constant velocity *v* is considered (Figure 5.6). The beam is simply supported at both ends. The cross-section is constant (Young modulus, *E*, Second moment of area, *I*, and damping coefficient, *c*) with uniform mass distribution (mass per unit length, μ). The formulation developed in this section will be taken as the basis for some of the dynamic Bridge WIM algorithms presented in the following chapter.

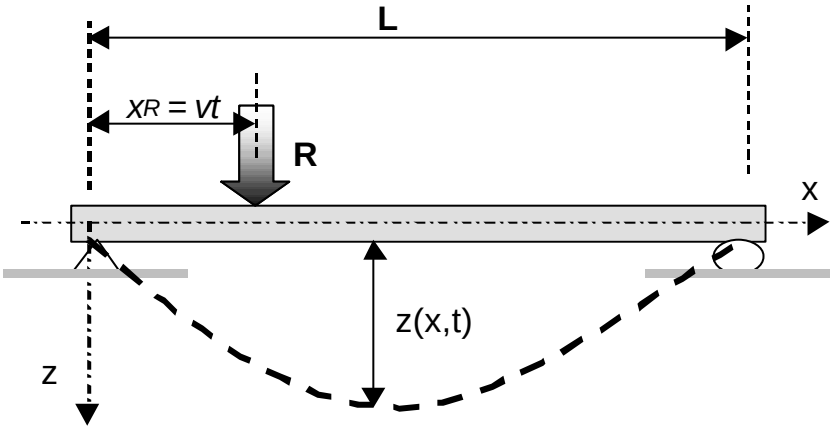

Figure 5.6 – Simply supported beam subjected to a constant moving force

The bridge deflection, *z(x,t),* can be expressed in terms of the modal coordinates, Z_i, and natural modes, $\Ö_i$, as given in Equation 5.16:

$$z(x,t) = \sum_{i=1}^{\infty} \Phi_i Z_i(t) \tag{5.16}$$

The equations of motion are derived directly from Lagrange's equations for each modal coordinate *i*:

$$\frac{d}{dt}\left(\frac{\partial K}{\partial \dot{\Phi}_i}\right) - \frac{\partial K}{\partial \Phi_i} + \frac{\partial V}{\partial \Phi_i} - \frac{\partial W_D}{\partial \Phi_i} - \frac{\partial W}{\partial \Phi_i} = 0 \tag{5.17}$$

where K is total kinetic energy of the system calculated using the masses and velocities of the system components (Equation 5.18), V is the total potential energy of the system computed from the relative displacements (Equation 5.19), W_D is the dissipation energy of the system obtained from the damping forces (Equation 5.20) and W is the total virtual work (Equation 5.21):

$$K = \frac{1}{2}\int_0^L \mu\left(\frac{\partial z}{\partial t}\right)^2 dx \tag{5.18}$$

$$V = \frac{1}{2}\int_0^L EI\left(\frac{\partial^2 z}{\partial x^2}\right)^2 dx \tag{5.19}$$

$$W_D = \frac{1}{2}\int_0^L c\left(\frac{\partial z}{\partial t}\right)dx \tag{5.20}$$

$$\delta W = -R\delta z \tag{5.21}$$

As a result of substituting Equations 5.18 to 5.21 into Lagrange's equation (5.17), the bending vibration of the beam, $z(x,t)$, is defined:

$$EI\frac{\partial^4 z(x,t)}{\partial x^4} + \mu\frac{\partial^2 z(x,t)}{\partial t^2} + 2\mu\omega_b\frac{\partial^2 z(x,t)}{\partial t^2} = \delta(x - x_R)R \tag{5.22}$$

where

$z(x,t)$: displacement of the bridge at position x and time t,

E, μ and I : Young's modulus, mass per unit length, and second moment of area of the bridge respectively,

δ : Dirac function,

$\omega_b = \frac{\xi\omega_1}{\sqrt{1-\xi^2}}$, where ξ is viscous damping factor ($\xi = \frac{c}{2\mu\omega_1}$) and ω_1 is circular natural frequency of the bridge ($\omega_1 = 2\pi f_1$),

R : applied force,

x_R = vt, is the distance of the force from the left support, where v is velocity.

The solution to Equation 5.22 is given by Frýba (1972):

$$z(x,t) = \frac{2RL^3}{\pi^4 EI} \sum_{i=1}^{\infty} \frac{\sin\left(\frac{i\pi x}{L}\right)}{i^2\left[i^2\left(i^2-\alpha^2\right)^2 + 4\alpha^2\beta^2\right]} \left\{ \begin{array}{l} i^2\left(i^2-\alpha^2\right)\sin(i\omega t) \\ -i\alpha\left[i^2\left(i^2-\alpha^2\right) - 2\beta^2\right]e^{-\omega_b t}\sin(\omega_i' t) \\ -2i\alpha\beta\left[\cos(i\omega t) - e^{-\omega_b t}\cos(\omega_i' t)\right. \end{array} \right\} \quad (5.23)$$

where

$$\omega = \pi v / L \quad (5.24)$$

$$\alpha = \frac{\pi v / L}{\omega_1} \quad (5.25)$$

$$\beta = \frac{\zeta}{\sqrt{1-\zeta^2}} \quad (5.26)$$

$$\omega_i' = \sqrt{\omega_i^2 - \omega_b^2} \quad (5.27)$$

For this case of moving constant force, the only vehicle parameter affecting the bridge dynamic response is speed. As bridges have relatively low damping, the critical speed (speed at which the maximum deflection in forced vibration occurs) takes place when the travel time of the moving load to cross the beam span is from 0.7 to 1.0 times the fundamental period of the bridge (Michaltsos et al. 1996, Frýba 1972). Bridge deflection will decrease as vehicles increase their speed over the critical level, and bridge response will get closer to the static response as vehicles decrease their speed below the critical speed.

Strains are given by $\varepsilon = -h_g \frac{\partial^2 z}{\partial x^2}$, where h_g is the distance from the strain location to the neutral axis of the section. By differentiating Equation 5.23 twice with respect to x, strains can be expressed as in Equation 5.28:

$$\varepsilon = \frac{h_g RL}{4EI}\sum_{i=1}^{\infty}\frac{\frac{8i^2}{\pi^2}\sin\left(\frac{i\pi x}{L}\right)}{i^2[i^2(i^2-\alpha^2)^2+4\alpha^2\beta^2]}\left\{\begin{array}{l} i^2(i^2-\alpha^2)\sin(i\omega t)-\dfrac{i\alpha\,[i^2(i^2-\alpha^2)-2\beta^2}{\sqrt{i^4-\beta^2}}e^{-\omega_b t}\sin(\omega_i' t) \\ -2i\alpha\beta\,[\cos(i\omega t)-e^{-\omega_b t}\cos(\omega_i' t) \end{array}\right\} \tag{5.28}$$

If velocity of the moving forces, v, is very small, $\alpha \approx 0$ in the equation above. Then the static strain of the beam for a force at position $x_R = vt$ is given by Equation 5.29:

$$\varepsilon_s = \frac{h_g RL}{4EI}\sum_{i=1}^{\infty}\frac{\frac{8}{\pi^2}\sin\left(\frac{i\pi x}{L}\right)\sin(i\omega t)}{i^2} \tag{5.29}$$

The dynamic component, ε_d, can be obtained by subtracting the static strain, ε_s, (as defined in Equation 5.29) from the total strain, ε (Equation 5.28). This dynamic strain is illustrated in Equation 5.30:

$$\varepsilon_d = \frac{h_g RL}{4EI}\sum_{i=1}^{\infty}\frac{\frac{8i^2}{\pi^2}\sin\left(\frac{i\pi x}{L}\right)}{i^2[i^2(i^2-\alpha^2)^2+4\alpha^2\beta^2]}\left\{\begin{array}{l} -i^2\alpha^2\sin(i\omega t) \\ -\dfrac{i\alpha\,[i^2(i^2-\alpha^2)-2\beta^2}{\sqrt{i^4-\beta^2}}e^{-\omega_b t}\sin(\omega_i' t) \\ -2i\alpha\beta\,[\cos(i\omega t)-e^{-\omega_b t}\cos(\omega_i' t) \end{array}\right\} \tag{5.30}$$

Total strain at a certain point in space and time can be expressed as the sum of a static and a dynamic component ($\varepsilon = \varepsilon_s + \varepsilon_d$). Hence, substituting from Equation 5.28 gives:

$$\varepsilon = \varepsilon_s + \frac{h_g RL}{4EI}\sum_{i=1}^{\infty}\frac{\frac{8i^2}{\pi^2}\sin\left(\frac{i\pi x}{L}\right)}{i^2[i^2(i^2-\alpha^2)^2+4\alpha^2\beta^2]}\left\{\begin{array}{l} -i^2\alpha^2\sin(i\omega t)-\dfrac{i\alpha\,[i^2(i^2-\alpha^2)-2\beta^2}{\sqrt{i^4-\beta^2}}e^{-\omega_b t}\sin(\omega_i' t) \\ -2i\alpha\beta\,[\cos(i\omega t)-e^{-\omega_b t}\cos(\omega_i' t) \end{array}\right\} \tag{5.31}$$

From beam theory, the static strain for a section at location x due to a load R located at x_R can be obtained from Equations 5.32 and 5.33:

$$\varepsilon_{0-x_R} = \frac{h_g}{EI}\frac{R(L-x_R)}{L}x \quad ; \; 0 \le x \le x_R \tag{5.32}$$

$$\varepsilon_{x_R-L} = \frac{h_g}{EI}\frac{Rx_R}{L}(L-x) \quad ; \; x_R \le x \le L \tag{5.33}$$

By substituting Equations 5.32 and 5.33 into Equation 5.31, the theoretical solution can be determined accurately with a smaller number *m* of mode shapes than the infinite number of Equation 5.28:

$$\varepsilon_{0-x_R} = \frac{h_g}{EI}\frac{R(L-x_R)}{L}x + \frac{h_g RL}{4EI}\sum_{i=1}^{m}\frac{\frac{8i^2}{\pi^2}\sin\left(\frac{i\pi x}{L}\right)}{i^2[i^2(i^2-\alpha^2)^2+4\alpha^2\beta^2]}\left\{\begin{array}{l} -i^2\alpha^2\sin(i\omega t) - \dfrac{i\alpha[i^2(i^2-\alpha^2)-2\beta^2}{\sqrt{i^4-\beta^2}}e^{-\omega_b t}\sin(\omega_i' t) \\ -2i\alpha\beta[\cos(i\omega t) - e^{-\omega_b t}\cos(\omega_i' t) \end{array}\right\}$$

$$0 \le x \le x_R \tag{5.34}$$

$$\varepsilon_{x_R-L} = \frac{h_g}{EI}\frac{Rx_R}{L}(L-x) + \frac{h_g RL}{4EI}\sum_{i=1}^{m}\frac{\frac{8i^2}{\pi^2}\sin\left(\frac{i\pi x}{L}\right)}{i^2[i^2(i^2-\alpha^2)^2+4\alpha^2\beta^2]}\left\{\begin{array}{l} -i^2\alpha^2\sin(i\omega t) - \dfrac{i\alpha[i^2(i^2-\alpha^2)-2\beta^2}{\sqrt{i^4-\beta^2}}e^{-\omega_b t}\sin(\omega_i' t) \\ -2i\alpha\beta[\cos(i\omega t) - e^{-\omega_b t}\cos(\omega_i' t) \end{array}\right\}$$

$$X_R \le x \le L \tag{5.35}$$

5.3.2 Multiple loads

In the case of a system of concentrated moving forces, $R_1, R_2, ..., R_n$, spaced at $a_1, a_2, ..a_{n-1}$, from the position of the first force and all travelling at speed *v*, the total virtual work due to the applied forces is given by:

$$\delta W = -\sum_{i=1}^{n}\varepsilon_i\delta(x-x_i)R_i\delta z_i \tag{5.36}$$

where

δ : Dirac function,

n : total number of forces,

ε_i = 1 when force i is on the bridge (otherwise zero),

R_i : value of constant force i,

x_i = $vt - a_i$, is the position of force i (the position of first force on the bridge is $x_1 = vt$), where a_i is spacing between first force and i^{th} force.

By substituting in Lagrange's Equation (5.17), the bending vibration ($z(x,t)$) of the beam at position x and time t will be given by:

$$EI\frac{\partial^4 z(x,t)}{\partial x^4} + \mu\frac{\partial^2 z(x,t)}{\partial t^2} + 2\mu\omega_d\frac{\partial^2 z(x,t)}{\partial t^2} = \sum_{i=1}^{n}\varepsilon_i\delta(x - x_i)R_i \tag{5.37}$$

The solution to Equation 5.37 is:

$$\varepsilon = \sum_{j=1}^{j=n}\frac{h_g\varepsilon_j\delta(x - x_j)R_jL}{4EI}\left[\sum_{i=1}^{\infty}\frac{\frac{8i^2}{\pi^2}\sin\left(\frac{i\pi x}{L}\right)}{i^2[i^2(i^2-\alpha^2)^2 + 4\alpha^2\beta^2]}\left\{\begin{array}{l} i^2(i^2-\alpha^2)\sin\left(i\omega(t-\frac{a_j}{v})\right) \\ -\frac{i\alpha[i^2(i^2-\alpha^2) - 2\beta^2}{\sqrt{i^4-\beta^2}}e^{-\omega_b t}\sin(\omega_i' t)\} \\ -2i\alpha\beta\,[\cos(i\omega t) - e^{-\omega_b t}\cos(\omega_i' t) \end{array}\right\}\right] \tag{5.38}$$

Hence, the principle of superposition applies when a system of constant forces moving on a bridge at uniform speed is considered.

5.4 RANDOM ROAD PROFILE MODEL

The unevenness of the road surface is an important factor that affects the dynamic response of bridge structures. Road irregularities and their input in a vehicle model are discussed in this section.

5.4.1 Definition of Road Roughness

To analyse the vehicle response, the road profile can be assumed to be a random process described by a power spectral density (PSD) function. The height of road irregularities (*r*) is generated from the formula (Yang & Lin 1995):

$$r(t) = \sum_{i=1}^{N} \sqrt{4S(\omega_i)}\Delta\omega \cos(\omega_i t - \theta_i) \tag{5.39}$$

where

$S(\omega_i)$: Power spectral density function ,

ω_i : Circular frequency (rad/s),

θ_i : Independent random variable uniformly distributed in the range from 0 to 2π.

N : Number of discrete frequencies.

Road profiles are different depending on the random numbers θ_i used in Equation 5.39. Attending to the classification of road roughness given by ISO (**I**nternational **S**tandards **O**rganisation) specifications, the PSD function for highway surface roughness is (Wong 1993):

$$\text{For} \quad \begin{cases} \omega \le \dfrac{1}{2\pi} cycle/m \Rightarrow S(\omega) = \dfrac{a}{(2\pi\omega)^2} \\ \omega > \dfrac{1}{2\pi} cycle/m \Rightarrow S(\omega) = \dfrac{a}{(2\pi\omega)^{1.5}} \end{cases} \tag{5.40}$$

Depending on the road conditions:

$$\begin{cases} a < 8x10^{-6} (very\_good) \\ 8x10^{-6} \le a < 32x10^{-6} (good) \\ 32x10^{-6} \le a < 128x10^{-6} (average) \\ 128x10^{-6} \le a < 512x10^{-6} (poor) \\ 512x10^{-6} \le a < 2048x10^{-6} (very\_poor) \end{cases}$$

where a (m^3/cycle) is the roughness coefficient (value of the spectral density at the discontinuity frequency $\frac{1}{2\pi}$). Appendix B gives an indication of what accuracy might be achievable from a WIM site with a measured IRI[17] (**I**nternational **R**oughness **I**ndex). Figure 5.7 relates the roughness coefficient, *a*, of the PSD function for $\omega \le \frac{1}{2\pi}$ and the IRI. An IRI of 6.0 is regarded as the minimum value for highways, which is equivalent to a

roughness coefficient of $a = 0.64(2\pi)^2 x10^{-6} = 25.3x10^{-6}$ m/cycle in Figure 5.7. Appendix B recommends a WIM site with an IRI lower than 2.6 mm/m for accuracy class B, that is, lower than $a = 0.1(2\pi)^2 x10^{-6} = 4x10^{-6}$ m/cycle (a 'very good' road profile according to Equation 5.40).

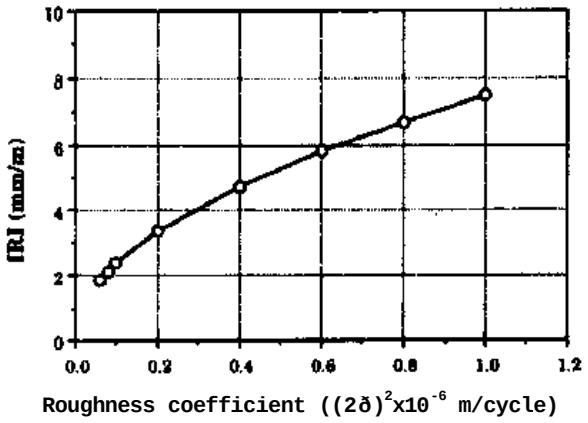

Figure 5.7 – Roughness coefficient of PSD versus IRI (after Hwang & Nowak 1991)

A portion of the theoretical vertical profile corresponding to a road in 'good' conditions ($a = 16x10^{-6}$ m/cycle, IRI ≅ 4.6 mm/m) is shown in Figure 5.8.

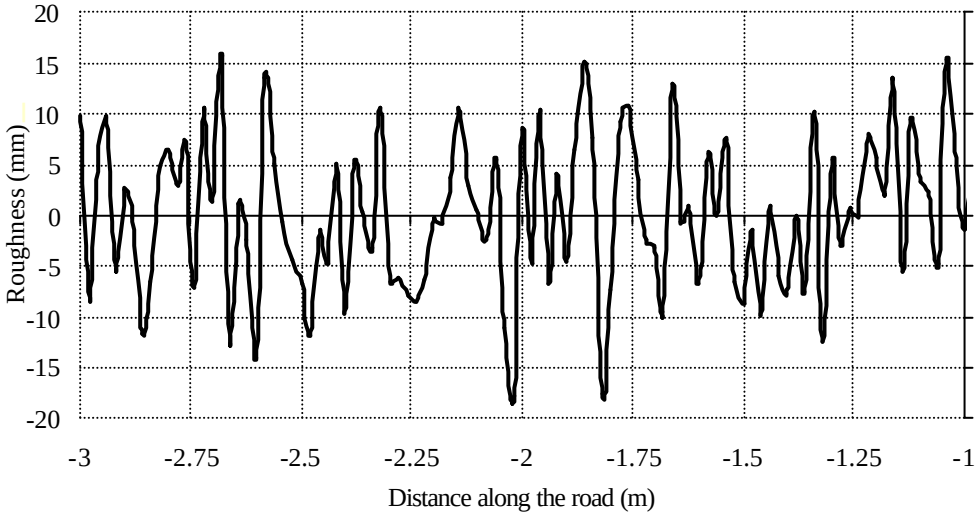

Figure 5.8 – Random road profile in 'good' conditions

The magnitude of the bridge response depends strongly not only on the unevenness of the road profile, but also on the velocity of the vehicles and the condition of the road leading to the bridge. The effects of occasional large irregularities such as potholes, misalignments at

the abutments or expansion joints have been removed in the previous analysis, but they can not be ignored and will be treated separately (Section 6.2.2). Though a B-WIM site with a smooth road profile improves accuracy, IRI does not properly account for the unevenness near the expansion joint (O'Brien et al. 1999b). Tests carried out on full-scale bridges have revealed that vehicles can cause excess stresses on bridges of 5 to 10% over smooth roads, 40 to 50% over poor bumpy roads, and 47 to 85% if there is an obstacle (impact effect) in the path of the wheel (Major 1980). Chompooming & Yener (1995) show how certain combinations of bump characteristic (i.e., height and length) and vehicle speed can result in very high dynamic effects.

5.4.2 Vehicle-Road profile interaction

An example of how to implement the road irregularities is presented next. Figure 5.9 represents a vehicle model composed of mass *M*, spring constant *K*, and damping coefficient *C*, moving at constant speed *v* along a road profile (vertical position *r(x)*).

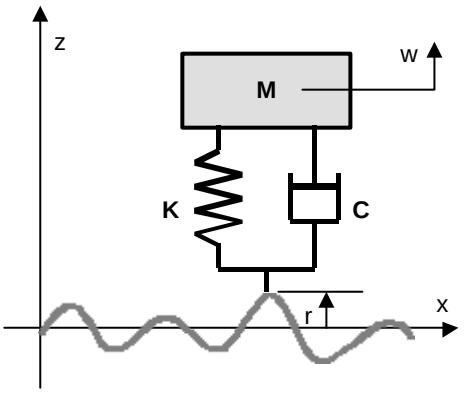

Figure 5.9 – Vehicle model moving on a road surface

The equation of motion for the vehicle model is given by Equation 5.41:

$$M\frac{d^2w}{dt^2} + C\left(\frac{dw}{dt} - \frac{dr}{dt}\right) + K(w - r) = 0 \qquad (5.41)$$

If $y = w - r$ then:

$$M\frac{d^2y}{dt^2}+C\frac{dy}{dt}+Ky=-M\frac{d^2r}{dt^2} \tag{5.42}$$

Since $r(x)$ is known, the vibration of the vehicle $w = r + y$ can be easily determined once the response y is solved for the given forcing function $\frac{d^2r(t)}{dt^2}$.This function represents the road profile $r(x)$ with $x = vt$. The road profile can be the result of measurements or a stochastic process as generated by Equation 5.39.

5.5 BRIDGE SUBJECTED TO A MOVING TWO-AXLE RIGID BODY

A planar two-axle body is implemented with the numerical methods proposed by Frýba (1972). Figure 5.10 shows the four degrees of freedom of the model, allowing for pitch and bounce of the truck body. A three dimensional model would be necessary to take roll motion into account, but the influence of roll on bridge dynamics has been proven to be small compared to that of pitch and vertical motions (Chompooming & Yener 1995). The vehicle parameters are: speed (v), axle spacing (D), body inertia (J), sprung mass ($m_s=m_{s1}+m_{s2}$), unsprung masses (m_{u1} and m_{u2}), tyre stiffness (K_{ti}), and damping (C_i) and (K_{si}) suspension stiffness at each axle. Compared to Equations 5.12 and 5.13, this simplified model assumes $C_t = 0$ and $F_s = 0$.

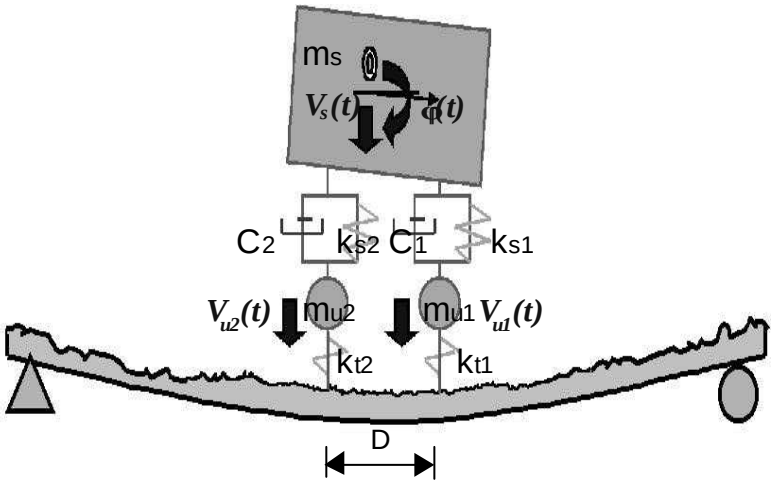

Figure 5.10 – Numerical simulation (Frýba model)

As introduced in Section 5.2.2, equations of motions are expressed by dynamic equilibrium of the different components of the structural system. Hence, Equation 5.43 defines the rotation (φ) of the sprung mass:

$$-J\frac{d^2\varphi(t)}{dt^2}+\sum_{i=1}^{2}(-1)^i\frac{m_s-m_{si}}{m_s}\{K_{si}[v_{ui}(t)-v_{si}(t)]+C_i[\dot{v}_{ui}(t)-\dot{v}_{si}(t)]\}=0 \tag{5.43}$$

where:

$$v_{si}(t)=v_s(t)-(-1)^i\frac{m_s-m_{si}}{m_s}\varphi(t) \tag{5.44}$$

and

v_s : Vertical displacement of sprung mass measured from the equilibrium position in which suspension springs are compressed by vehicle static mass,

v_{ui} : Vertical displacement of unsprung mass *i* measured from the position in which tyre springs are undeformed,

φ : Rotation of sprung mass measured in the clockwise direction from the horizontal.

Equation 5.45 represents the vertical motion (v_s) of the sprung mass:

$$-m_s\frac{d^2v_s(t)}{dt^2}-\sum_{i=1}^{2}\{K_{si}[v_{ui}(t)-v_{si}(t)]+C_i[\dot{v}_{ui}(t)-\dot{v}_{si}(t)]\}=0 \tag{5.45}$$

Equations 5.46 represent the vertical motions (v_{u1} and v_{u2}) of both unsprung masses:

$$m_{ui}g+m_{si}g-\frac{m_{ui}d^2v_{ui}(t)}{dt^2}+K_{si}[v_{ui}(t)-v_{si}(t)]+C_i[\dot{v}_{ui}(t)-\dot{v}_{si}(t)]-R_i(t)=0\ ;\ i=1,2 \tag{5.46}$$

Equation 5.47 provides an expression for the bending vibration (*z(x,t)*) of the beam,

$$EI\frac{\partial^4 z(x,t)}{\partial x^4}+\mu\frac{\partial^2 z(x,t)}{\partial t^2}+2\mu\omega_b\frac{\partial z(x,t)}{\partial t}=\sum_{i=1}^{2}\varepsilon_i\delta(x-x_i)R_i(t) \qquad (5.47)$$

where

$z(x,t)$: Displacement of the bridge at position x and time t,

E, μ and I : Young's modulus, mass per unit length, and second moment of area of the bridge respectively,

δ : Dirac function,

ε_i = 1 when axle i is on the bridge (otherwise zero),

ω_b = $\frac{\xi\omega_1}{\sqrt{1-\xi^2}}$, where ξ is viscous damping factor ($\xi = \frac{c}{2\mu\omega_1}$) and ω_1 is circular natural frequency of the bridge ($\omega_1 = 2\pi f_1$),

$R_i(t)$: Interaction force between the bridge and the applied axle force i,

x_i = $vt - a_i$, is the position of axle i (the position of first axle is $x_1 = vt$), where a_i is spacing between first axle and i^{th} axle, and v is velocity,

x_1 = vt and $x_2 = vt - D$ are the axle positions.

$R_i(t)$ is the applied axle i force at the point of contact on the beam and it is related to the rest of the vehicle by Equation 5.46. These forces, $R_i(t)$, are time-dependent, as the position of the axles change with time and the suspension of the vehicle oscillates due to irregularities of the bridge deck and bridge vertical displacement under tyres. Equation 5.48 takes into account the effect of bridge displacement and road profile on the interaction forces:

$$R_i(t) = K_{ti}[v_{ui}(t) - z(x_i,t) - r(x_i)] \quad ; \quad i = 1,2 \qquad (5.48)$$

Frýba (1972) reduces this set of five differential equations (5.43 to 5.48) to a dimensionless form that can be readily solved by the method of finite Fourier integral transformation. Computer code has been developed by the author to solve the final differential equations of second order using the Runge-Kutta method (Appendix E). The program allows the user to specify bridge parameters (stiffness, length, mass), truck parameters (masses, suspension and tyre properties, speed, axle spacings) and a stochastic (Section 5.4) or a measured road profile (code included in CD-ROM accompanying thesis).

The interaction between the vehicle and the bridge can be included through the iterative procedure shown in Figure 5.11.

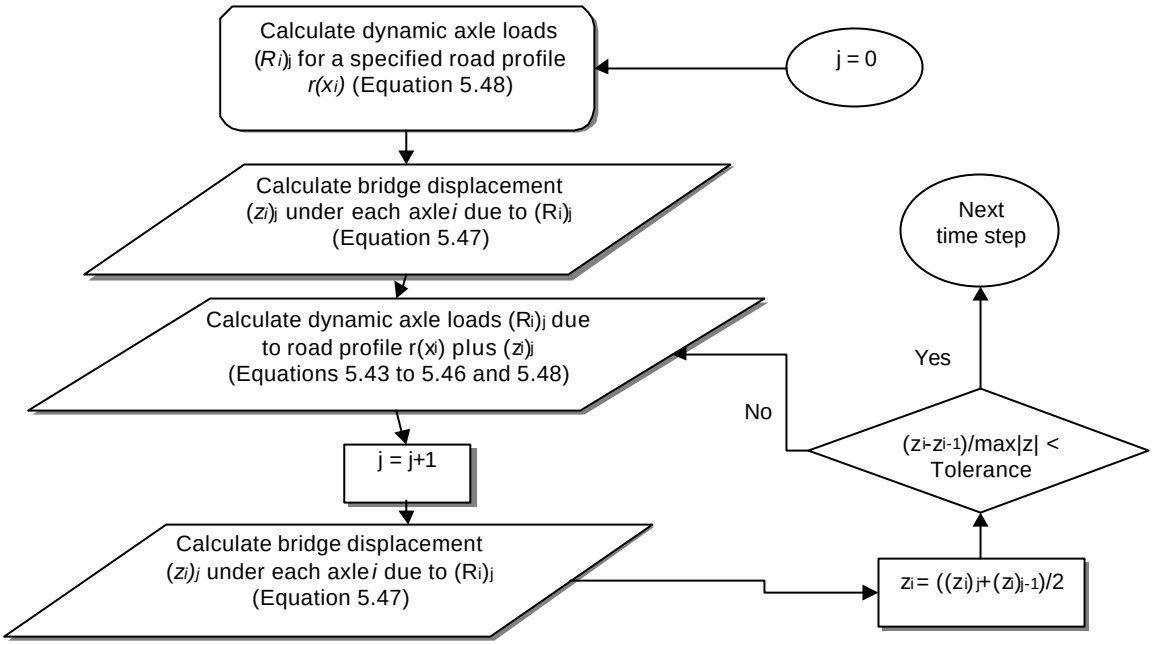

Figure 5.11 – Iteration technique for solving interaction at each time step

Preliminary studies on the bridge response have been carried out with only one iteration from the algorithm shown in Figure 5.11. In order to study the impact of a change in the truck dynamic parameters, some values are adopted as reference: speed 20 m/s, static load 58836 N on each axle, pitching inertia 50×10^3 kgm^2, axle spacing 4 m, tyre stiffness 700×10^3 N/m, suspension stiffness 80×10^3 N/m, and suspension damping 7×10^3 Ns/m at each axle. The characteristics of the bridge model are: span 20 m, mass (μ) 25.5×10^3 kg/m, flexural rigidity (EI) 3×10^{10} Nm^2, first natural frequency 4.26 Hz, critical damping 1%, and 'good' road conditions (a = 16x10^{-6}), unless otherwise specified.

5.5.1 Effect of Bridge Characteristics

From a B-WIM point of view, individual axle weights are easier to identify for shorter bridge lengths (i.e. culverts). However, the average applied axle force might be far from the static value if the bridge length and/or vehicle speed does not allow for a few dynamic oscillations. Therefore, a high excitation of truck dynamics by a road irregularity prior to the bridge might not have time to be damped out by the vehicle damping mechanisms. A

longer bridge allows for the recording and averaging of more readings, but the separation of the effect of a single axle from others might be more difficult (i.e., due to low vehicle/bridge mass ratio). Additionally, simultaneous traffic events are more likely to take place as the bridge length increases.

In medium to long span bridges, bridge-truck interaction can be estimated by a quarter car model with two mass elements being the bridge and gross vehicle mass (these two degrees of freedom represent the body bounce frequency and bridge natural frequency). OECD (1997) reports significant coupling for a modal bridge mass 20 times greater than the vehicle mass. This is not the case for short span bridges where the length of the truck might be greater than the bridge span, in which case bridge vibration is due to axle hop modes on the vehicle, rather than body bounce modes. Strong damping (>2%) can limit the dynamic response of short span bridges significantly (Chompooming & Yener 1995). Damping of longer bridges is less important.

Figure 5.12 shows the strain response at midspan due to the passing of the two-axle truck taken as reference for three different bridge lengths: 10, 20 and 40 m with natural frequencies of 17.04, 4.26 and 1.06 Hz respectively.

on the bridge response as a whole, statics and dynamics are mixed at very low frequencies and their separation might involve the loss of some static component.

5.5.2 Effect of Truck Parameters

Applied dynamic axle forces tend to get higher with increasing speed. When the vehicle is on the bridge, the behaviour of the truck changes due to the bridge deflection. Figures 5.13(a) and (b) represent the force-position history for the front axle prior to and on the bridge respectively. It does not appear to be a dominant frequency due to the road roughness, but the amplitude of the oscillations is slightly bigger on the bridge.

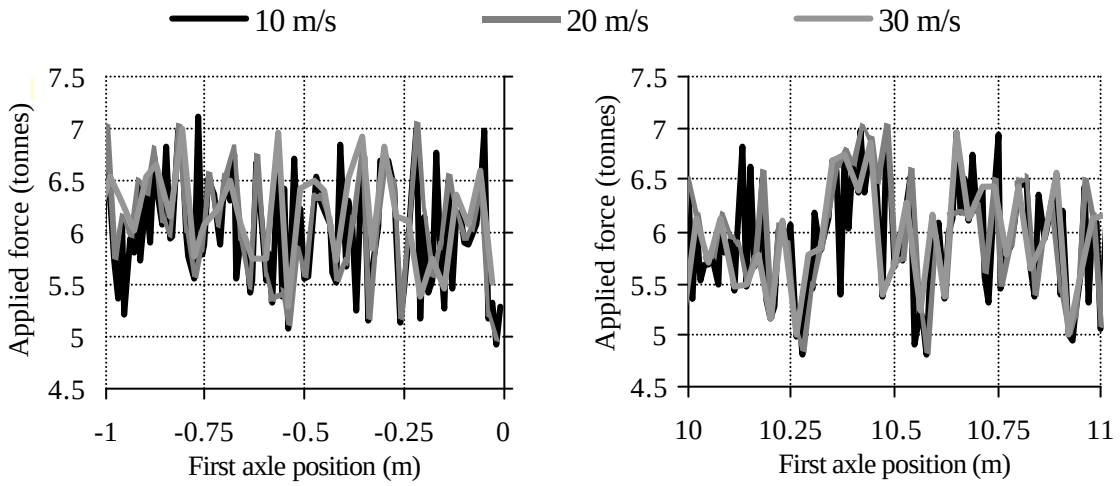

(a) Dynamic load prior to the bridge (b) Dynamic load on the bridge

Figure 5.13 - Influence of speed on applied axle forces

Bridge dynamic response increases with speed up to 20 m/s as shown in Figure 5.14(a). The spectrum of the total strain response reveals the influence of the first natural frequency of the bridge, 4.2 Hz, at 20 m/s (Figure 5.14(b)).

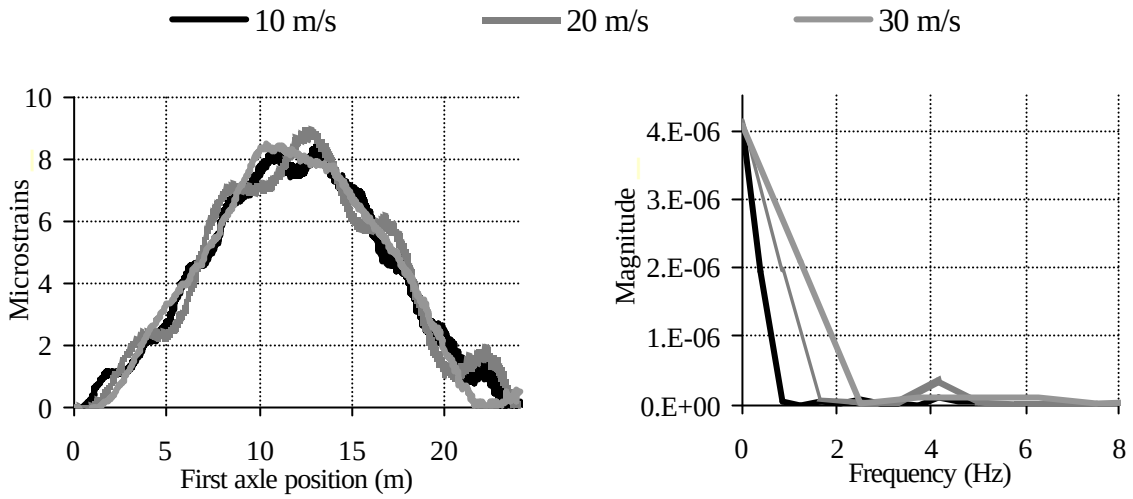

(a) Strain measurements (b) Spectrum of the strain signal

Figure 5.14 - Influence of speed on bridge response

There are a wide variety of truck mechanical characteristics that can cause different bridge responses. A 10 m short span bridge, mass 12×10^3 kg/m, flexural rigidity 2.7×10^9 Nm^2, first natural frequency of the bridge in flexure 7.45 Hz and critical damping 5% is used for testing. The road conditions are considered 'very good' (a = $4x10^{-6}$). An increase/decrease in pitching inertia by 20% around the reference values did not induce significant changes in the bridge response. When suspension damping is increased by 20%, bridge response is slightly smaller. Truck frequencies change when masses on the vehicle change. Hence, higher dynamic amplification might result from lighter trucks depending on the frequency matching with the bridge.

In the case of Figure 5.15(a), the bridge response is approximately proportional to the change in mass and there is no coupling. Figure 5.15(b) represents the bending response due to an increase/decrease of 20% around the reference value for tyre stiffness. An increase in tyre stiffness causes a higher response: This can be due to a very low frequency that does not have enough time to go through a full cycle along the bridge or to the interaction of axle hop and bridge frequencies.

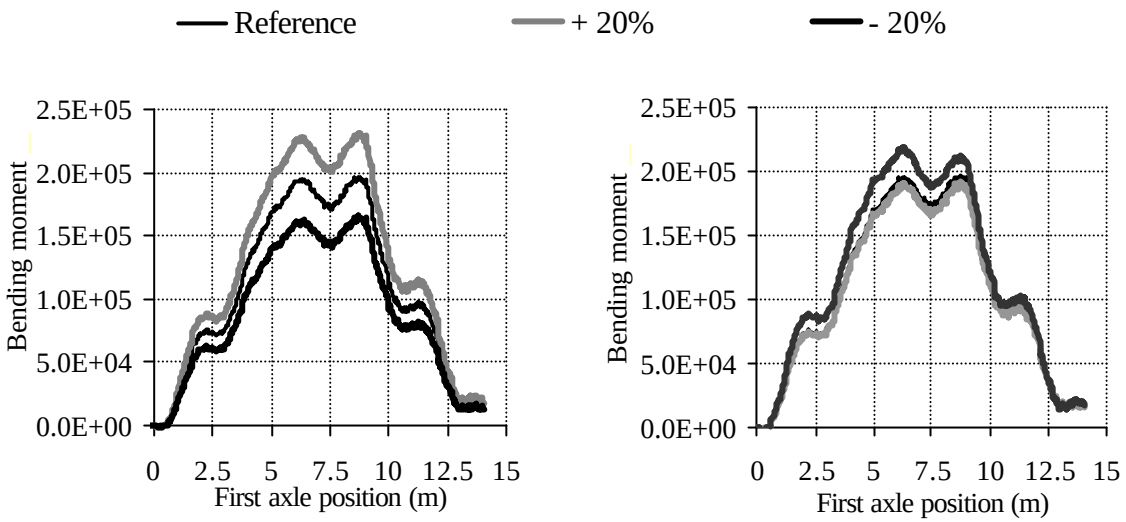

(a) Body mass (b) Tyre stiffness

Figure 5.15 – Effect of a change in body mass / tyre stiffness

In conclusion, if a truck is passed over a structure with the same masses, but different mechanical characteristics, bridge response can differ for each run. If these differences exhibit a significant deviation from the expected static response, the site might not be suitable for a high-accuracy B-WIM system.

5.6 EFFECT OF SUSPENSION TYPE AND ROAD ROUGHNESS

Through a collaboration with Green (Queen's University, Kingston, Canada), the author secured the dynamic bridge responses for heavy vehicles with steel-spring and air-spring suspensions and found the influence of suspension type on Bridge WIM accuracy. The bridge and truck are modelled separately and combined in an iterative procedure. The method involves convolution of the vehicle loads with modal responses of the bridge and the convolution integral is solved by transformation to the frequency domain using the fast Fourier transform. The method is then extended by an iterative procedure to include dynamic interaction between the bridge and an arbitrary mathematical model of a vehicle. Green & Cebon (1994) illustrate the effectiveness of this calculation method, the convergence of the iterative procedure and the good agreement with experimental data.

The vehicle models developed by Green et al (1995) are a steel sprung four-axle articulated vehicle validated experimentally, and a similar vehicle fitted with air suspensions and

hydraulic dampers. The dynamic response of a 30 m beam model is obtained for crossings of each of these two vehicles. The four-axle articulated vehicle has 11 degrees of freedom as shown in Figure 5.16. In this Figure, elements A (non-linear behaviour), B (Coulomb friction) and C (linear spring/damper) represent springs in Figures 5.4(c), (b) and (a) respectively.

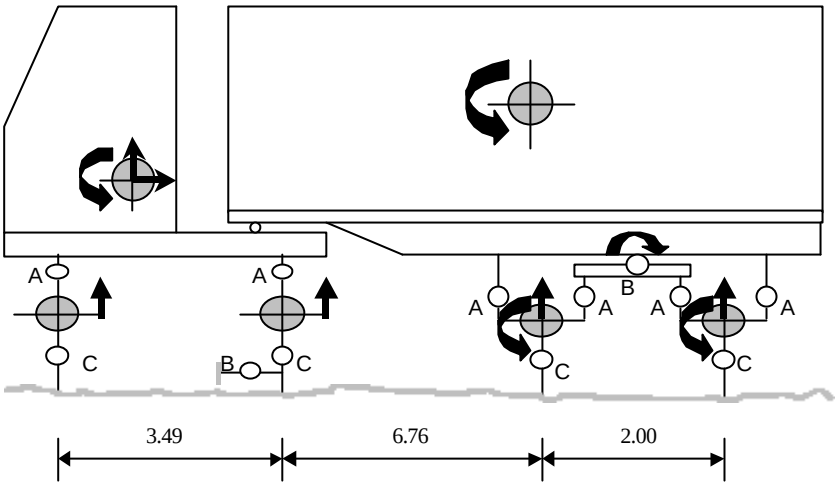

Figure 5.16 – Two dimensional tractor and trailer vehicle model with steel-spring suspensions (11 degrees of freedom)

For the vehicle with air suspension, models of air springs with parallel viscous dampers replace the steel-spring elements on the drive axle and the two trailer axles. The suspension on the steer axle is the same for both vehicle models. Two surface profiles, three different speeds (55, 70 and 85 km/h) and three different loading conditions are chosen for the simulations.

Figures 5.17 and 5.18 represent the applied dynamic forces over same length of smooth and rough road profile respectively.

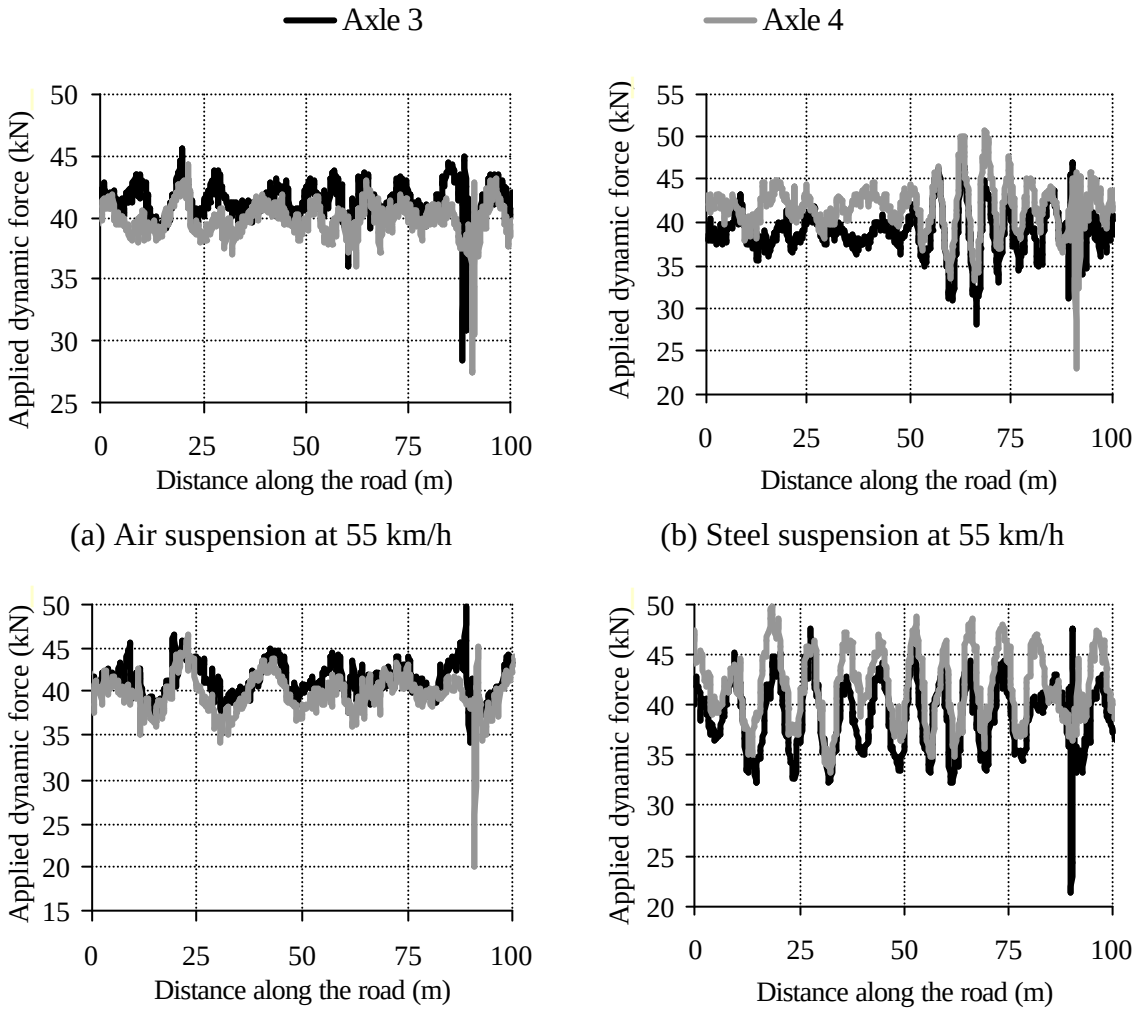

Figure 5.17 – Applied forces by air- and steel-sprung fully laden tandem (smooth profile)

It can be seen how these forces increase with speed and road roughness. Steel suspensions are clearly more sensitive to these changes, except for a singularity localised at about 90 m at the speed of 85 km/h. Generally, the dynamic response is lower for the air suspension than for the steel suspension vehicle as the air suspensions are better damped and the vehicle dampers absorb energy from the bridge vibrations. The load sharing between axles within the tandem of the air-sprung vehicle is also less than in the steel-sprung vehicle.

The amplitude of the applied dynamic wheels is higher for worse road conditions as shown in Figure 5.18. Thus, bridge response will increase with road roughness. Therefore, body bounce modes of vehicle vibration are excited by longer wavelength variations in road profile whereas axle hop are excited by short wavelength defects such as pot-holes, road

debris, a rough repair or a mis-aligned joint in a bridge, more likely to occur in a road in poor conditions.

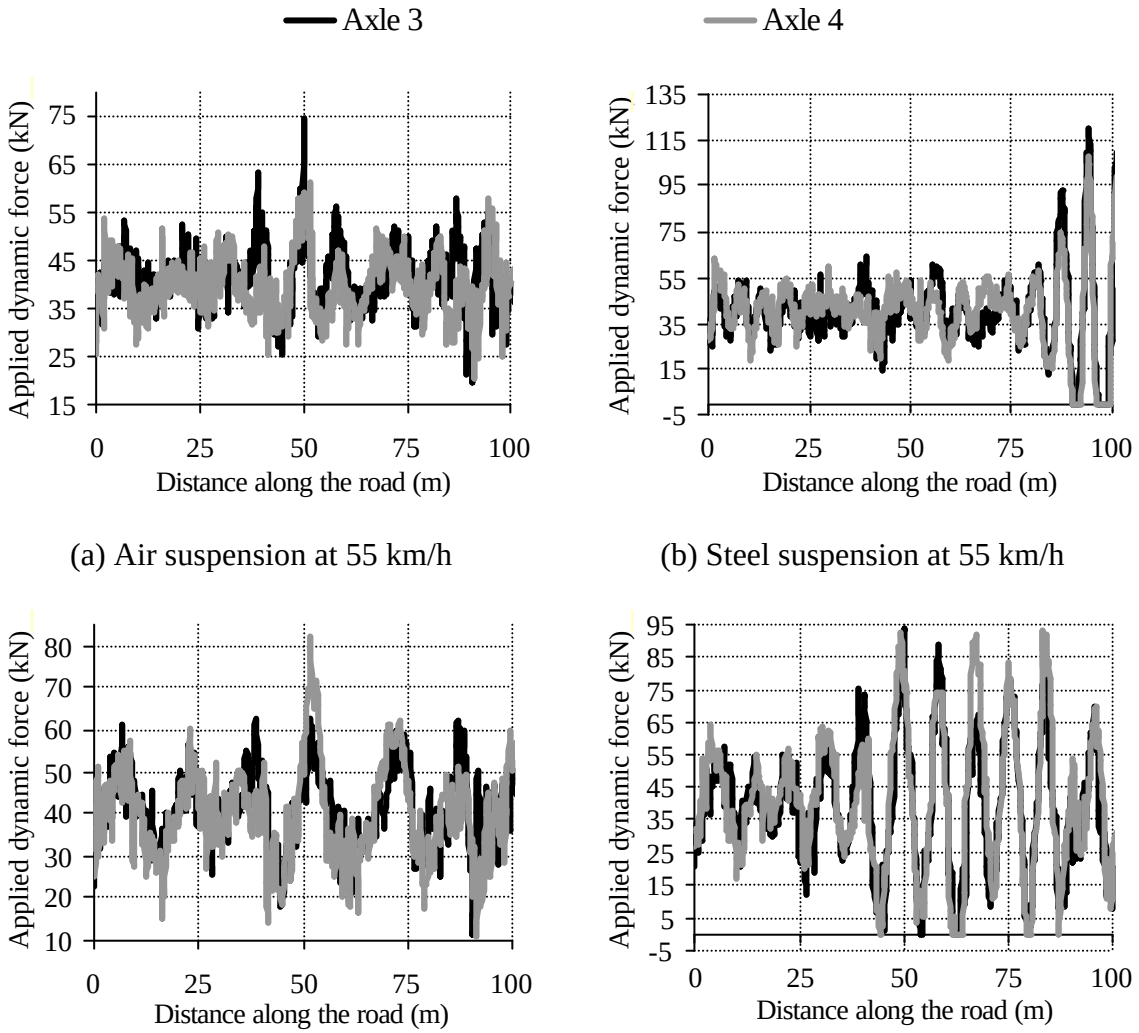

(a) Air suspension at 55 km/h

(b) Steel suspension at 55 km/h

(b) Air suspension at 85 km/h

(c) Steel suspension at 85 km/h

Figure 5.18 – Applied forces by air- and steel-sprung fully laden tandem (rough profile)

The air-sprung vehicle has lower natural frequencies than the steel-sprung vehicle. Figures 5.19 and 5.20 shows the Discrete Fourier Transform for the second axle travelling at 70 km/h in unloaded and fully laden conditions respectively. There is not a dominant frequency for the air suspension vehicle in Figure 5.19(a) due to the heavy damping. This damping will minimise dynamic response even in the case of a bridge with low natural frequency and likely frequency matching. From Figure 5.19(b), the dynamic component of the truck at 3.38 Hz is very significant for the steel suspension.

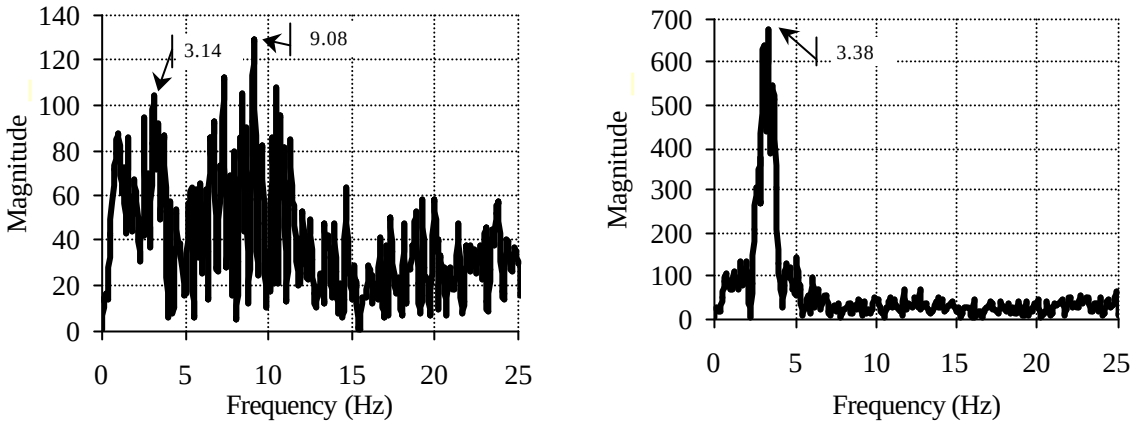

(a) Air suspension (b) Steel suspension

Figure 5.19 – Spectra analysis of 2rd axle in unloaded vehicle (70 km/h)

The increase of mass for the laden vehicle of Figure 5.20 decreases the value of the main natural frequencies. Therefore, the influence of air suspension damping is less important in heavier vehicles. Even so, the applied dynamic load by an air-suspension vehicle is still small.

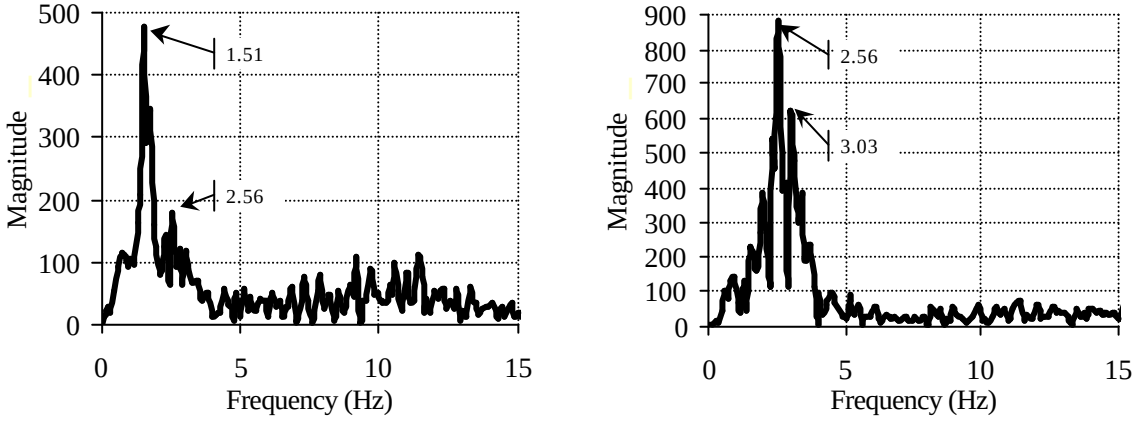

(a) Air suspension (b) Steel suspension

Figure 5.20 – Spectra analysis of 2rd axle in fully laden vehicle (70 km/h)

The Discrete Fourier Transforms of the force applied by all axles in the tractor and trailer for the fully laden vehicle are presented in Figure 5.21. Tractor and trailer bounce takes place at 1.51 Hz in the air suspension vehicle and 2.56 Hz in the steel suspension vehicle.

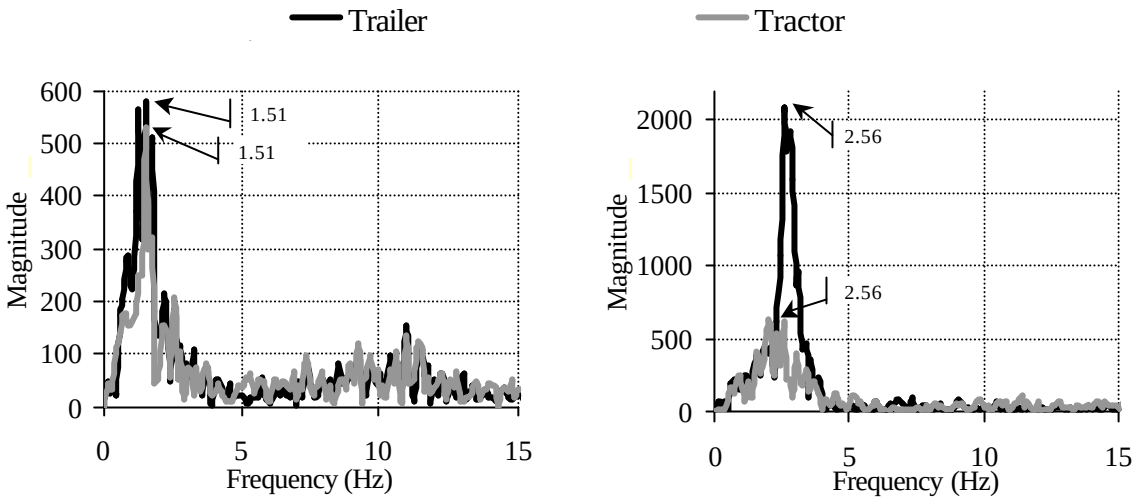

(a) Air suspension (b) Steel suspension

Figure 5.21 – Spectra of sum of axle forces for fully laden vehicle (70 km/h)

The Discrete Fourier Transforms of the difference in axle forces for the tractor and trailer are presented in Figure 5.22. A tractor and trailer pitch of 2.56 Hz is displayed by the air suspension vehicle, while a tractor and trailer pitch of 3.03 and 3.14 Hz respectively the steel-sprung vehicle.

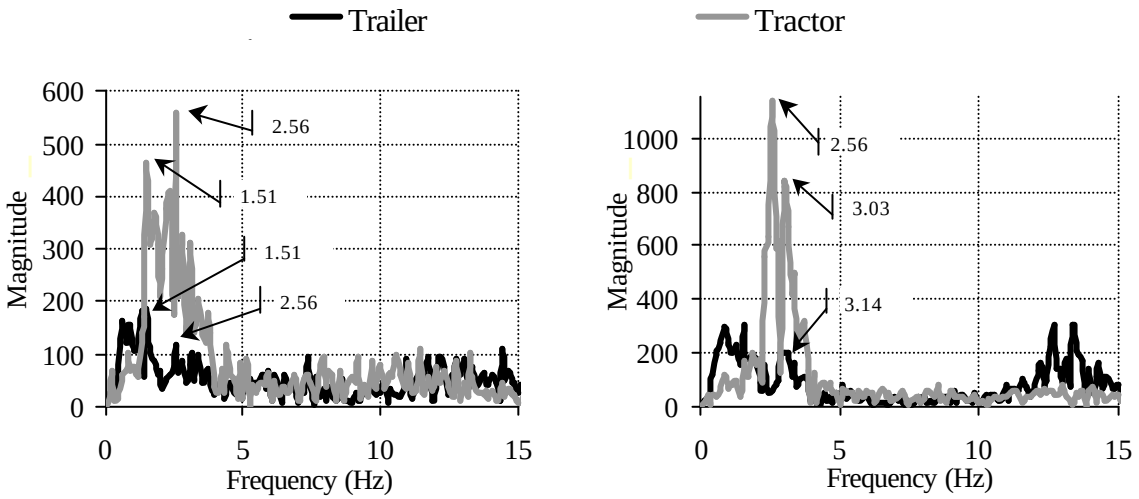

(a) Air suspension (b) Steel suspension

Figure 5.22 – Spectra of difference of axle forces for fully laden vehicle (70 km/h)

The strain response at the bridge midspan for a fully laden vehicle on a smooth profile is represented in Figure 5.23. As expected, steel suspension causes higher dynamic oscillations on strain than air-suspension vehicles.

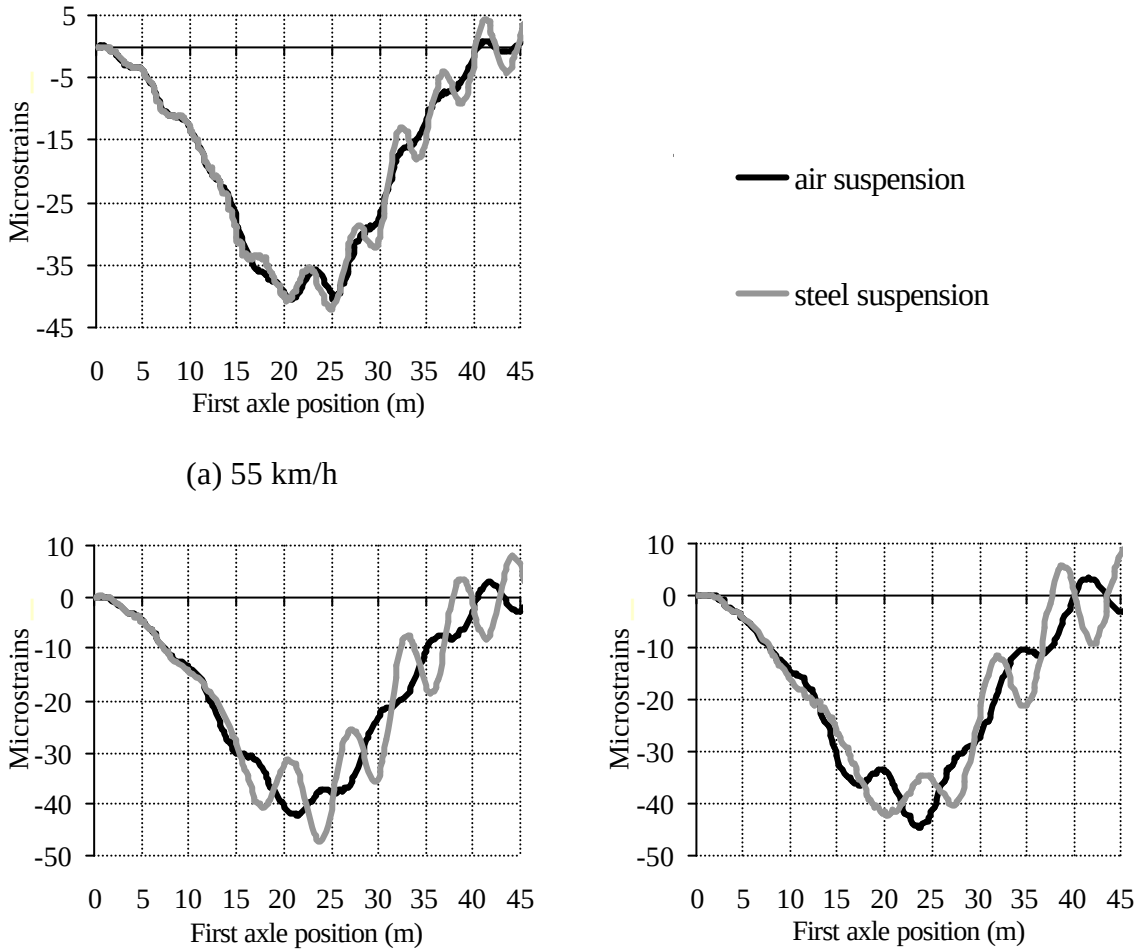

Figure 5.23 - Effect of speed on a smooth profile

Figure 5.24 shows the bridge response at midspan for the fully laden vehicle on a rough profile. The maximum dynamic response takes place at 70 km/h for the steel-sprung vehicle and 85 km/h for the air-sprung vehicle. It can be seen that the air-suspended vehicle causes significantly lower dynamic bridge response than the steel-spring suspended vehicle and it is less sensitive to a change in speed. In comparison to the smooth profile, the dynamic response due to the steel-sprung vehicle increases by over 100%. These high dynamics suggest the occurrence of frequency matching between the steel-sprung vehicle and the bridge. Consequently, Bridge WIM will tend to be less accurate in the cases of steel-spring suspensions, rough road profile, for this bridge, for vehicle speeds near 70 km/h.

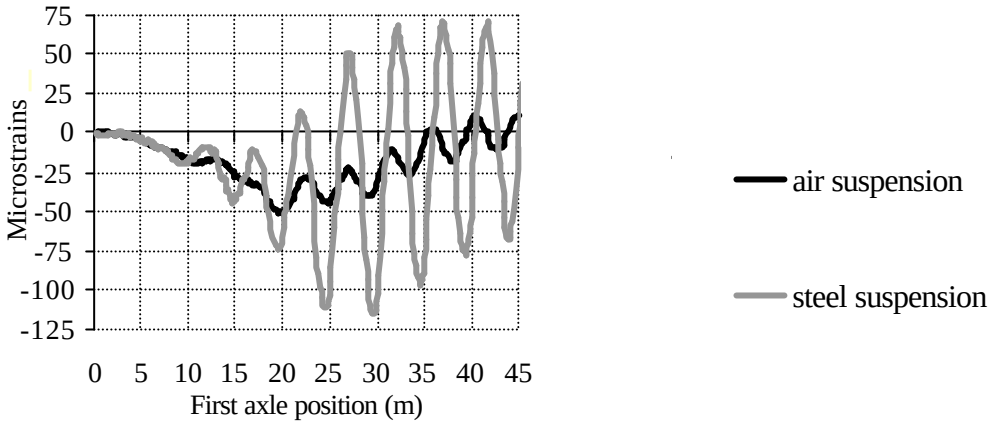

(a) 55 km/h

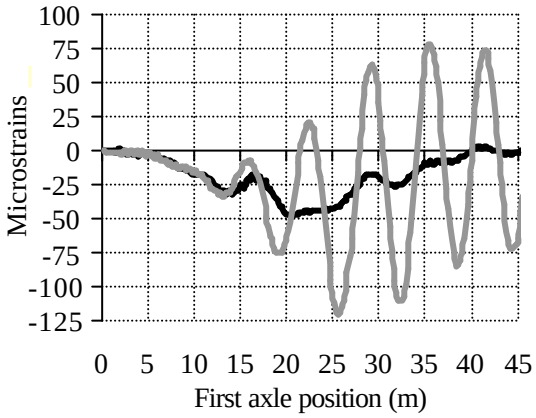

(b) 70 km/h

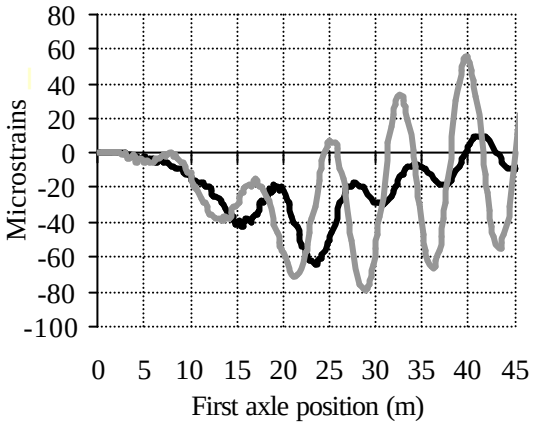

(c) 85 km/h

Figure 5.24 - Effect of speed on a rough profile